Total Number and Mean Size of Alveoli in Mammalian Lung Estimated Using Fractionator Sampling and Unbiased Estimates of the Euler Characteristic of Alveolar Openings

D.M. HYDE,[1]* N.K. TYLER,[1] L.F. PUTNEY,[1] P. SINGH,[1] AND H.J.G. GUNDERSEN[2]

[1]California National Primate Research Center, University of California, Davis, California

[2]Stereological Research Laboratory, University of Aarhus, Århus, Denmark

ABSTRACT

Estimation of alveolar number in the lung has traditionally been done by assuming a geometric shape and counting alveolar profiles in single, independent sections. In this study, we used the unbiased disector principle to estimate the Euler characteristic (and thereby the number) of alveolar openings in rat lungs and rhesus monkey lung lobes and to obtain robust estimates of average alveolar volume. The estimator of total alveolar number was based on systematic, uniformly random sampling using the fractionator sampling design. The number of alveoli in the rat lung ranged from $17.3 \cdot 10^6$ to $24.6 \cdot 10^6$, with a mean of $20.1 \cdot 10^6$. The average number of alveoli in the two left lung lobes in the monkey ranged from $48.8 \cdot 10^6$ to $67.1 \cdot 10^6$ with a mean of $57.7 \cdot 10^6$. The coefficient of error due to stereological sampling was of the order of 0.06 in both rats and monkeys and the biological variation (coefficient of variance between individuals) was 0.15 in rat and 0.13 in monkey (left lobe, only). Between subdivisions (left/right in rat and cranial/caudal in monkey) there was an increase in variation, most markedly in the rat. With age (2−13 years) the alveolar volume increased 3-fold (as did parenchymal volume) in monkeys, but the alveolar number was unchanged. This study illustrates that use of the Euler characteristic and fractionator sampling is a robust and efficient, unbiased principle for the estimation of total alveolar number in the lung or in well-defined parts of it. Anat Rec Part A 274A:216–226, 2004. © 2004 Wiley-Liss, Inc.

Key words: alveoli; biological variation; disector; Euler characteristic; fractionator; monkey; stereology; rat

The airways of the human lung are composed of a series of branching tubes with about 16 generations of conducting airways from the trachea to the terminal bronchiole that decrease in diameter distally. The terminal respiratory unit, defined as all the alveolar ducts together with their alveoli that arise from the most proximal respiratory bronchiole, comprises on the average generations 17–23 (Weibel, 1963). Airway diameter remains almost unchanged with each generation in the terminal respiratory unit and thereby the total airway cross section nearly doubles with each generation, a feature that favors O_2 diffusion. Because gas molecules diffuse much faster in a gas than in a water phase, the true limitation to gas diffusion is through the wall of the air–blood membrane and into the red blood cells. Weibel (1970) developed a morphometric model of pulmonary diffusion capacity that

Grant sponsor: NIEHS; Grant number: P01 ES-00628; Grant sponsor: NCRR; Grant number: RR000169.

*Correspondence to: Dallas M. Hyde, California National Primate Research Center, One Shields Avenue, University of California, Davis, CA 95616. Fax: (530) 752-0420. E-mail: dmhyde@primate.ucdavis.edu

Received 21 March 2003; Accepted 3 September 2003

DOI 10.1002/ar.a.20012

© 2004 WILEY-LISS, INC.

was inversely related to the thickness of the air–blood membrane, but directly related to the surface area of the interalveolar septa. Consequently, alveolar number and development of interalveolar septa are critical factors in pulmonary diffusion. It has been indicated that a substantial number of pulmonary alveoli are formed after birth in most species (~90% in humans) where saccules are subdivided by the outgrowth and elongation of septa from their walls (Thurlbeck, 1975; Burri, 1984). As a result of this critical window in postnatal growth, practical procedures, based on unbiased principles for estimating alveolar number in the lung, are essential for documenting disruption of normal alveolar development.

Over the past few decades, there has been an evolution of rigorously uniform sampling designs in stereology that allow unbiased estimates of number, length, surface area, and volume. This approach has been termed "design-based" stereology because of the reliance on actual sampling designs rather than virtual, geometric model-based stereology (Gundersen et al., 1988a,b).

The estimation of alveolar number in the lung has traditionally been done by assuming a specific geometric shape (Weibel and Gomez, 1962). However, geometric assumption-based estimates of alveolar number in the human lung have been shown to underestimate alveolar number, as evaluated by human acinar reconstructions (Hansen and Ampaya, 1975). These investigators identified six rather different geometric shapes in their acinar reconstructions. This diversity of alveolar shapes illustrates the problem of assuming a particular geometric shape for pulmonary alveoli. More recent approaches to estimating alveolar number have used serial reconstruction of a small number of alveoli per lung (Mercer et al., 1994) or a selector method of estimating alveolar volume (Massaro and Massaro, 1996) and dividing the mean alveolar volume into the volume density of alveoli per lung to derive the number of alveoli per lung. However, this is a very elaborate and indirect method fraught with statistical error from a small sample size and undefined biases in volume estimation: In a single section, most alveolar profiles do not have a closed boundary, which makes the accurate estimation of individual volume impossible.

We used the fractionator (Gundersen, 1986, 2002), a rigorous sampling approach to entire rat lungs and monkey lung lobes, and the Euler characteristic of the net of alveolar openings to estimate without bias the total number of alveoli in these anatomically well-defined lungs and lung lobes. Our results illustrate that using the Euler characteristic with fractionator sampling is very efficient and does not require knowledge of tissue shrinkage in the estimation of total alveolar number in the lung. In addition, the sampling design illustrates that the fractionator may effortlessly be combined with other sampling requirements, like a specific orientation distribution of the sections and estimates of global volume shrinkage, necessary for robust estimates of surface area and length of lung structures.

MATERIALS AND METHODS

Unbiased Estimation of the Number of Alveolar Openings

Anatomical structure. The last branch of the tracheobronchial tree is the terminal bronchiole, which is the primary airway that opens into terminal respiratory units

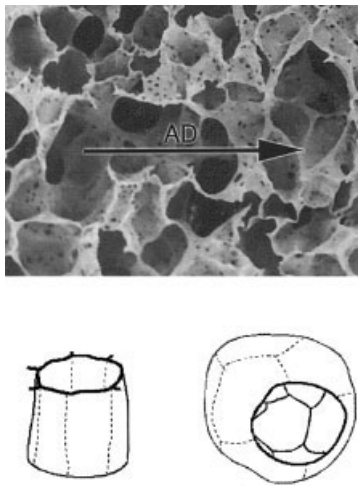

Fig. 1. Alveolar duct (AD, arrow) with clearly defined individual alveolar openings is evident in this portion of a terminal respiratory unit seen in scanning electron microscopy. An alveolus is sketched in the lower left with its opening (heavy line) and the attachment of the walls of neighboring alveoli indicated (dotted lines). The illustration to the lower right shows a view from the terminal bronchiole into the terminal respiratory unit air space, where alveolar openings can be seen at the far end. The drawn, continuous surface separates the terminal respiratory unit from all its alveoli in 3D: the surface is a continuous patchwork of all alveolar openings and rests on the complete upper rim of the alveolar walls. In this (virtual) surface, the complete set of all alveolar openings forms a 2D net with a 3D shape of a bag.

comprised of respiratory bronchioles, alveolar ducts, and alveoli (Fig. 1). The walls of pulmonary alveoli are very irregular, honeycomb-like surface specializations of the inner surface of the terminal respiratory unit and alveoli are thus not isolated in any ordinary sense. The alveolar walls are continuous with each other (structurally, in each acinus there is only one alveolar surface), and the interior of an alveolus (the empty air space) is continuous with the air space of the remainder of the terminal respiratory unit (which, in turn, is continuous with that of the tracheobronchial tree and the environment). It is this anatomical structure that makes ordinary number estimation impossible because there are no isolated, individual alveoli in a geometric or topological sense.

It is very easy, however, to see individual, distinct alveolar features using, e.g., scanning electron microscopy of lung tissue (Fig. 1). Pathways of alveolar ducts and alveolar openings are clearly visible individually and might easily be counted directly in 3D, but there are several almost insurmountable obstacles for making such a procedure quantitative. For the purpose of this study, we therefore adopt the ordinary definition of one alveolus: the dead-end air space unambiguously identified by the alveolar opening and limited by a part of the alveolar wall.

As indicated in Figure 1, there is no problem in formulating an anatomical and topological model that describes reality for this structure. The virtue of the topological model, a simple 2D net of alveolar openings at the rim of the alveolar wall, is that it allows the use of unbiased principles as a basis for ordinary stereological quantitation. As detailed below, the disector (Sterio, 1984) is an unconditionally unbiased probe for sampling of topological

15524892, 2004, 1, Downloaded from https://anatomypubs.onlinelibrary.wiley.com/doi/10.1002/ar.a.20012, Wiley Online Library on [17/04/2025]. See the Terms and Conditions (https://onlinelibrary.wiley.com/terms-and-conditions) on Wiley Online Library for rules of use; OA articles are governed by the applicable Creative Commons License

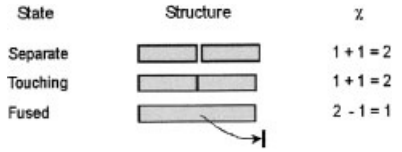

Fig. 2. Additivity of the Euler characteristic. Two iron bars have $\chi = 2$, whether separated or touching. To make them into one, single bar, an (abstract) "separator" of $\chi = 1$ must be removed, as indicated by the χ-arithmetic of the universe of all bars (right). After fusion of the two bars into one, the local universe contains fewer objects, which must be reflected in its Euler characteristic. Note that in the mathematical symbolism of manipulating the Euler characteristic of sets of objects, an abstract "separator" is not needed; it is used here for purely didactic purposes.

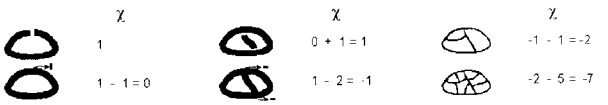

Fig. 3. Making and measuring of 2D nets. To the left, a bar joins itself, and its Euler characteristic is therefore reduced from $\chi = 1$ to $\chi = 0$ by removal of the separator. The fusion of a new structuring element of $\chi = 1$, with the ring of $\chi = 0$, generates a little net of $\chi = -1$ after removal of 2 separators, as shown in the middle. To the right, the generation of a 2D net is shown wherein a total of 7 extra connections have been added. The total number of holes in the net is 8.

events, and the practical counting of these events, happening at the end of the profiles of alveolar walls in thin sections, is surprisingly easy and robust.

Definition of the Euler characteristic of 2D nets. The method developed for estimation of the number of alveolar openings is based on the mathematical concept of the so-called Euler characteristic of structure. The Euler characteristic, χ, reports the topological complexity of structure of any dimension (Gundersen et al., 1993). It is an integer number but, unlike the ordinary counting measure, it may be positive, zero or negative—just like the bottom line of an account balance. When something positive is added, the balance becomes larger; when something positive is taken away, the balance shrinks and may become negative. A topologically simple structure like a 2D line segment or a 3D stone has an Euler characteristic of 1. So for simple, isolated things like a pile of sand or cells in the liver, the ordinary number of things and the Euler characteristic of the structure is the same.

As illustrated in Figure 2, the Euler characteristic is a strictly additive measure, just as volume and ordinary number, and additivity is a feature sine qua non for quantitation. This leads to a somewhat unfamiliar set of rules for measuring and changing the topology of structure. It is also a consequence of the additivity that the Euler characteristic of complex structure, like a network, may be hugely negative, as indicated in the making of a 2D net in Figure 3.

The net generated in Figure 3 has 8 holes and an Euler characteristic of $\chi = -7$. The relation between the number of holes in such a 2D net and its Euler characteristic is very simple:

$$\mathrm{N(holes)} = 1 - \chi \qquad (1)$$

Fig. 4. Counting Islands and Bridges in 2D nets with the physical disector. The net in the middle is intersected by a stack of disectors seen edge-on. All local topological differences in the disectors are counted. If a new profile is seen in a disector field (nothing in the other field) an Island is counted; all cases shown to the left. If one profile is seen as two separate profiles in the other field, a Bridge is counted, as shown to the right. Using Eqs. 1 and 3 in the text, the unbiased estimate of the number of holes is $\mathrm{N(holes)} := 1 - (\Sigma I - \Sigma B)/2 = 1 - (-4)/2 = 3$.

where N indicates that the total number is the ordinary counting measure. The relation is in complete agreement with common sense: It takes one element to outline the first hole; $-\chi$ is the number of extra connections. Eq. 1 holds for each 2D net of alveolar openings in each acinus, wherein the number of alveoli is of the order 10^2–10^3. Ignoring the constant "1" per acinus, we obtain the simple estimator

$$\mathrm{N(holes)} := -\chi \qquad (2)$$

which may underestimate the total number of alveoli by a fraction of 0.01–0.001, which we shall ignore for the present purpose. The notation ":=" indicates that this is an estimator, not a mathematical identity (like Eq. 1).

Disector estimation of the Euler characteristic of 2D nets. The reason for the above derivation, which might look like a detour to get at the number of alveolar openings, is that it would not be efficient to use the disector principle for unbiased estimation of the number of potentially very irregular holes in a 2D net. In contrast, from a mathematical point of view, the disector is primarily an unbiased sampling probe of the Euler characteristic, although it is much better known as a counting probe for isolated objects.

When estimating the Euler characteristic of a 2D net using the disector, all occurrences of the two possible local topological differences, Islands and Bridges, between the two sections are counted, as illustrated in Figure 4. An Island, I, is counted when a new isolated or locally unconnected profile appears in the disector. If a connection is made between two locally separate profiles in a field, a Bridge, B, is counted. The unbiased estimate of the contribution, $\Delta\chi$, to the Euler characteristic in a disector is

$$\Delta\chi = (\,I - B\,)/2 \qquad (3)$$

where the divisor of 2 compensates for the (efficient) counting of both ways in the disector (inefficient one-way counting would be counting only Islands and Bridges in the left field, say).

The real 2D net of alveolar openings is suspended in 3D space and at a first glance looks very different from the above when observed in thin sections. The footprint of an

15524892, 2004, 1, Downloaded from https://anatomypubs.onlinelibrary.wiley.com/doi/10.1002/ar.a.20012, Wiley Online Library on [17/04/2025]. See the Terms and Conditions (https://onlinelibrary.wiley.com/terms-and-conditions) on Wiley Online Library for rules of use; OA articles are governed by the applicable Creative Commons License

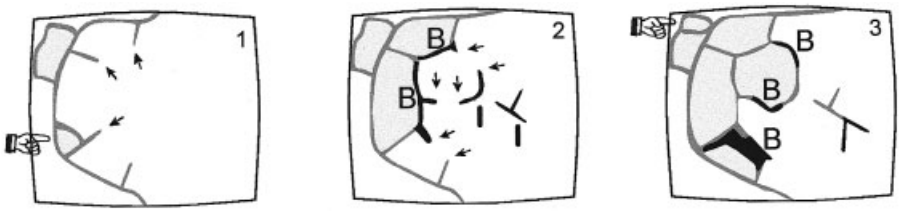

Fig. 5. Counting Islands and Bridges in 2D nets in 3D space with the physical disector illustrated by a series of sections of lung tissue. The 2D net of alveolar openings is only represented by the free ends of the alveolar walls. New wall structure in a section compared to the previous one is shown in black, arrows point to free ends that become connected by Bridges (B) in the next section, and new Islands (in practice a rare event) are indicated by I. The pointers indicate new alveolar (bottom) profiles, which are not counted, because no free ends are involved. One of the new Islands in the second field becomes larger and changes shape in the third section, but topologically it is still one isolated profile and nothing is counted. The width of the large profile of a Bridge in the last field indicates that, locally, the wall is almost parallel to the section.

TABLE 1. Constants of the fractionator sampling design in rat total lung and monkey left lung, respectively*

Species	sf(bar)	sf(block)	h(dis) (mm)	BW (mm)	sf(height) (h/BW)	dx, dy (mm)	a(fra) (mm^2)	sf(area) (a/dx/dy)	SF	$\Sigma\Delta\chi$
Rat	0.32	0.47	0.009	3.95	0.0023	0.84	0.028	0.044	$1.3 \cdot 10^{-5}$	239
Monkey	0.25	0.38	0.01	12.1	0.00095	1.23	0.19	0.14	$5.3 \cdot 10^{-5}$	295

*Cf. also text.

alveolar openings in a section is the two free ends of alveolar walls. Only changes in the disector of the topology of the free ends count, as illustrated in Figure 5.

As for ordinary number, the estimation of the Euler characteristic may be performed in physical disectors using the classical density $\times$V(ref) setup, with monitoring and correction of global shrinkage, or using the fractionator, where shrinkage may be ignored. For this study, we used the fractionator (Table 1).

Animals

Four male and one female rhesus macaques (*Macaca mulatta*, California National Primate Research Center at UC Davis) and five male Wistar rats (Jackson Laboratories) were used for this study. The monkeys ranged in age from 28 to 157 months and in body weight from 3.4 to 11.6 kg (cf. Table 2), were born at the California National Primate Research Center, and their medical records were known and considered in their selection. All monkeys were given a comprehensive physical examination, including a chest radiograph and complete blood count, and were determined to be healthy monkeys. Monkeys were anesthetized with ketamine (30–35 mg/kg) administered subcutaneously and were killed with a pentobarbital sodium overdose in accordance with the Animal Care Guidelines of the California National Primate Research Center (Davis, CA). Rats were all retired breeders with the age not given and varied in body weight from 503 to 625g (Table 3). The animals were maintained on a 12:12-hr light/dark photoperiod and provided Purina Rodent Laboratory Chow 5001 (Purina Mills, St. Louis, MO) and water ad libitum. Animal studies conformed to applicable provisions of the Animal Welfare Act and other federal statutes and regulations relating to animals (Guide for the Care and Use of Laboratory Animals; National Institutes of Health, 1985).

Tissue Preparation

Lung fixation. Both monkey and rat lungs were instillation fixed at 30 cm H_2O pressure with Karnovsky's fixative (Karnovsky, 1965) diluted 50:50 with 4% low melting point agarose (FMC BioProducts, Rockland, ME, Cat #50161, melting point less than 65°C, gel temperature 26–30°C) solution for a 50% Karnovsky's and 2% agarose solution diluted in PBS. A syringe was filled with warm agarose fixative mixture (~40°C). The estimate of the mean alveolar volume (see later) is valid for the lung tissue with the distension resulting from the above instillation fixation.

Rat. The lungs were removed from the chest and fixed via the trachea by infusing the fixative mixture slowly into the lungs. The lungs were filled until fully expanded to the edges of the lobes at 30 cm H_2O pressure. After filling the lungs with fixative, they were tied off and allowed to fix overnight in Karnovsky's fixative. The heart, vessels and esophagus were dissected from the lungs and airways, and the total lung volume estimated by its buoyant weight in saline (Scherle, 1970). Following whole lung volume measurement, the lungs were separated at the hilus, tied off at the main bronchi, and each half-lung volume estimated.

Monkey. The whole monkey lungs were removed at necropsy and lobes were tied off and separated. For this study, the left cranial and left caudal lobes were fixed in the same manner as the rat lungs.

Sampling

The estimation of alveolar number, described above, may be performed with any orientation distribution of the uniformly sampled sections. In many studies of lung, one would, however, be interested in estimates of areas of various surfaces and lengths of vessels and airways, in addition to the number of alveoli. For both species, the lung tissue was therefore embedded according to an isotropic, uniformly random (IUR) protocol using the orientator (Mattfeldt et al., 1990; Gundersen et al., 1988a). The sampling and processing consequently also included steps necessary for monitoring and correcting shrinkage in estimates of other quantities, but the fractionator design for just total alveolar number estimation is independent of

15524892, 2004, 1, Downloaded from https://anatomypubs.onlinelibrary.wiley.com/doi/10.1002/ar.a.20012, Wiley Online Library on [17/04/2025]. See the Terms and Conditions (https://onlinelibrary.wiley.com/terms-and-conditions) on Wiley Online Library for rules of use; OA articles are governed by the applicable Creative Commons License

TABLE 2. Estimates of total number of alveoli and total volumes in left lung of monkey

							Parenchymal volume			Cumulative alveolar volume			No. of alveoli			Mean alveolar volume		
Animal	Sex	Body weight (kg)	Age (mo)	Lobe Cr (cm^3)	Volume Ca (cm^3)	L. lobes (cm^3)	Cr par. (cm^3)	Ca par. (cm^3)	L. lobes par. (cm^3)	Cr alv. (cm^3)	Ca alv. (cm^3)	L. lobes alv. (cm^3)	Cr (10^6)	Ca (10^6)	L. lobes (10^6)	Cr (10^6 μm^3)	Ca (10^6 μm^3)	L. lobes (10^6 μm^3)
M1	M	3.4	28	45	72	117	41	70	111	16.3	33.8	50	25.8	41.5	67.1	0.63	0.81	0.74
M4	F	5.8	76	74	120	194	71	104	174	49.8	69.0	119	23.2	34.6	57.8	2.15	1.99	2.06
M6	M	3.85	96	70	93	163	67	88	154	49.3	53.3	103	25.9	22.9	48.8	1.90	2.33	2.10
M5	M	11.64	138	109	141	250	101	125	226	44.8	70.8	116	26.0	36.6	62.6	1.72	1.94	1.85
M3	M	6.05	157	129	190	319	124	185	309	60.2	92.8	153	21.3	30.9	52.3	2.82	3.00	2.93
Mean		6	99	85	123	209	81	114	195	44.1	63.9	108.0	24.5	33.3	57.8	1.8	2.0	1.9
CV		0.53	0.52	0.39	0.37	0.38	0.40	0.39	0.39	0.37	0.34	0.35	0.09	0.21	0.13	0.43	0.39	0.40
Avg CV						0.38			0.39			0.36			0.16			0.41

Cr, cranial lobe; Ca, caudal lobe; Par, parenchyma; Alv, alveoli; CV, coefficient of variation (SD/mean); AvgCV, CV of individual lobes.

TABLE 3. Estimates of total number of alveoli and total volumes in rats

		Lung volume			Parenchymal volume			Cumulative alveolar volume			No. of alveoli			Mean alveolar volume		
Animal	Body weight (g)	RL (cm^3)	LL (cm^3)	Lung (cm^3)	RL par. (cm^3)	LL par. (cm^3)	Lung par. (cm^3)	RL alv. (cm^3)	LL alv. (cm^3)	Lung alv. (cm^3)	RL (10^6)	LL (10^6)	Lung (10^6)	RL (10^6 μm^3)	LL (10^6 μm^3)	Lung (10^6 μm^3)
R5	503	10.6	8.8	19.4	10.2	8.2	18.4	6.4	4.1	10.5	13.5	4.4	17.9	0.47	0.94	0.71
R3	528	8.0	4.2	12.2	7.3	3.8	11.1	3.5	2.3	5.8	14.3	7.5	21.8	0.25	0.30	0.27
R4	573	11.4	5.5	16.9	10.9	5.1	16.1	5.7	2.5	8.2	11.2	13.4	24.6	0.51	0.19	0.35
R1	595	10.2	5.3	15.5	9.3	4.8	14.1	5.7	2.5	8.2	8.3	9.0	17.3	0.68	0.28	0.48
R2	625	12.3	6.1	18.4	10.4	5.7	16.1	6.4	3.5	9.8	12.5	6.2	18.7	0.51	0.55	0.53
Mean	565	10.5	6.0	16.5	9.6	5.5	15.2	5.5	3.0	8.5	11.9	8.1	20.1	0.5	0.5	0.5
CV	0.09	0.15	0.29	0.17	0.15	0.30	0.18	0.21	0.26	0.22	0.20	0.42	0.15	0.32	0.67	0.36
Avg CV				0.23			0.23			0.24			0.33			0.53

RL, right lobe; LL, left lobe. For abbreviations, see Table 2.

15524892, 2004, 1, Downloaded from https://anatomypubs.onlinelibrary.wiley.com/doi/10.1002/ar.a.20012, Wiley Online Library on [17/04/2025]. See the Terms and Conditions (https://onlinelibrary.wiley.com/terms-and-conditions) on Wiley Online Library for rules of use; OA articles are governed by the applicable Creative Commons License

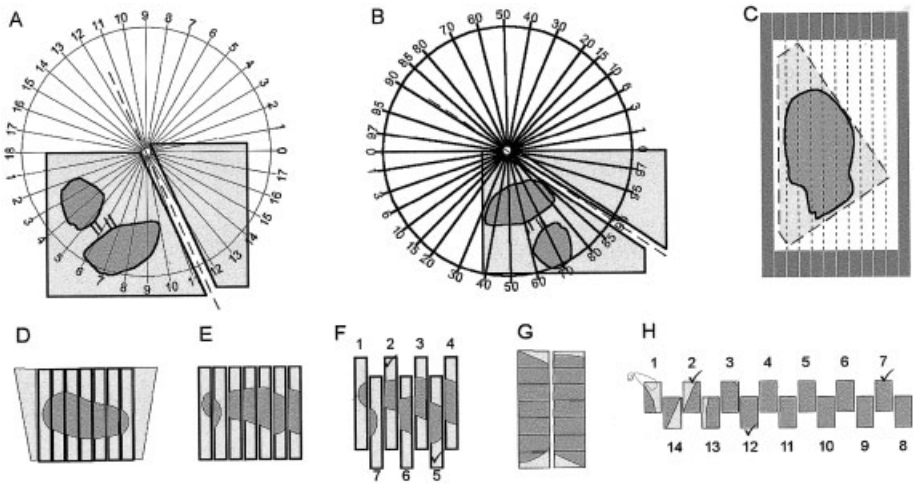

Fig. 6. IUR, smooth fractionator sampling. **A:** Agar-embedded lung placed on a uniform clock so that the cut along a uniformly random direction can be made in the agar, not in the tissue. The agar block is then made to rest on the face just cut; the 90°-edge is now in the 0-0 direction of the nonuniformly divided clock (**B**). Using a new random number, the cut is again made in the agar. The resulting block is re-embedded in the slicing machine with the last cut face parallel to the cutting direction of the slicing machine (**C**). Slabs are cut at a known, constant thickness. Each slab is then cut into bars of a width identical to the slab thickness (**D**; the cutting machines were obtained from J. Damm, Denmark at jdammvip@cybercity.dk). All bars are sorted according to the area of the upper surface (**E**), and every second is pushed a bit out of the row, providing the smooth fractionator sampling sequence, shown in **F**; all bars from all slabs are arranged in one sequence, the illustration shows only those from one slab. The decisive step in the smooth fractionator is that now the blocks are renumbered from the smallest to the largest in the upper row and further on to the smallest-but-one in the lower row. A sampling period, p, is chosen; a uniformly random starting number r is selected ($1 \le r \le p$); and the bars numbered r, r+p, r+2p$\cdots$ in the smooth sequence are sampled ($p = 3$ in the illustration in F, $r = 2$, and $r+p = 5$). The sampling period is the inverse sampling fraction. The sampled bars (tick marks) are cut perpendicularly to the axis at a length different from the width (G). The resulting blocks are again sorted with respect to the upper cut surface area and are rearranged and renumbered according to the smooth fractionator (H). Blocks are sampled with a period of $p = 5$; in the example the blocks numbered 2, 7, 12 are sampled (tick marks). Blocks are embedded without rotation such that IUR disector sections are cut from their upper surface.

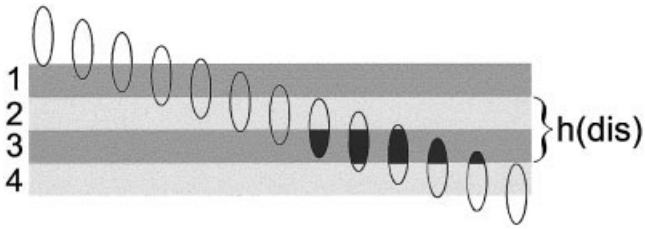

Fig. 7. Disector height, h(dis), in a series of sections where nonadjacent ones are used for counting features larger than the section separation. The sampling section is 3, the look-up section is 1 in the example. All events (particles) seen in the sampling section (black) are counted, provided they are not seen in the look-up section. The range of positions (of the top of the feature, say) where a count is made is the distance between two homonymous surfaces of the sampling and the look-up sections (twice the section thickness in the example).

any shrinkage, and the robust estimate of mean alveolar volume is independent of global shrinkage.

Rat

Embedding and slicing. Lungs were dried thoroughly and dipped in 4% ordinary agar at 80°C at least 3 times to ensure that the lungs were well coated with agar. Care was taken to get agar into all fissures and between the lobes of the rat right lung. Each half of the rat lung was immersed in warm 4% agar (55°C). The lobes were embedded perpendicularly to each other (one lung lying flat and the other standing on the diaphragmatic surface) in order to obtain as many different isotropic directions as possible. The block of agar containing the lung was allowed to harden overnight at 4°C to improve its cutting properties. The lungs were encased in enough agar so that there was extra "empty" agar for slicing during the next orientation steps. Each embedded lung was placed on a uniform clock (Fig. 6), a random number between 1 and 18 was selected, and a cut was made in the agar along the numbered line on the clock and perpendicular to the table. The cut surface was placed on a sine-weighted clock, and the edge of the cut surface was aligned with the 0-0 line. A uniformly random number between 1 and 97 was selected, and a cut, also perpendicular to the table, was made along that direction. After the last cut, which is an IUR section plane, the lung was placed into a slicing machine such that all subsequent cuts were parallel to the IUR plane. The slicing machine was filled with warm agar which was allowed to harden overnight at 4°C.

The lung block was sliced with a uniformly random start at a thickness (usually 5 mm) selected to obtain ~10 slices of lung tissue. The slices (always including a scale) were photographed with a Nikon Coolpix 950 camera (Melville, NY); this step is only relevant for shrinkage estimation for other estimators. The slabs were then sliced into bars at the same thickness as the slabs (i.e., the bars have a quadratic cross section). The bars were subsampled with the fractionator (Fig. 6), and 10 bars were selected using a random start from a random number table. The lengths of the bars were cut to a different dimension than that pre-

15524892, 2004, 1, Downloaded from https://anatomypubs.onlinelibrary.wiley.com/doi/10.1002/ar.a.20012, Wiley Online Library on [17/04/2025]. See the Terms and Conditions (https://onlinelibrary.wiley.com/terms-and-conditions) on Wiley Online Library for rules of use; OA articles are governed by the applicable Creative Commons License

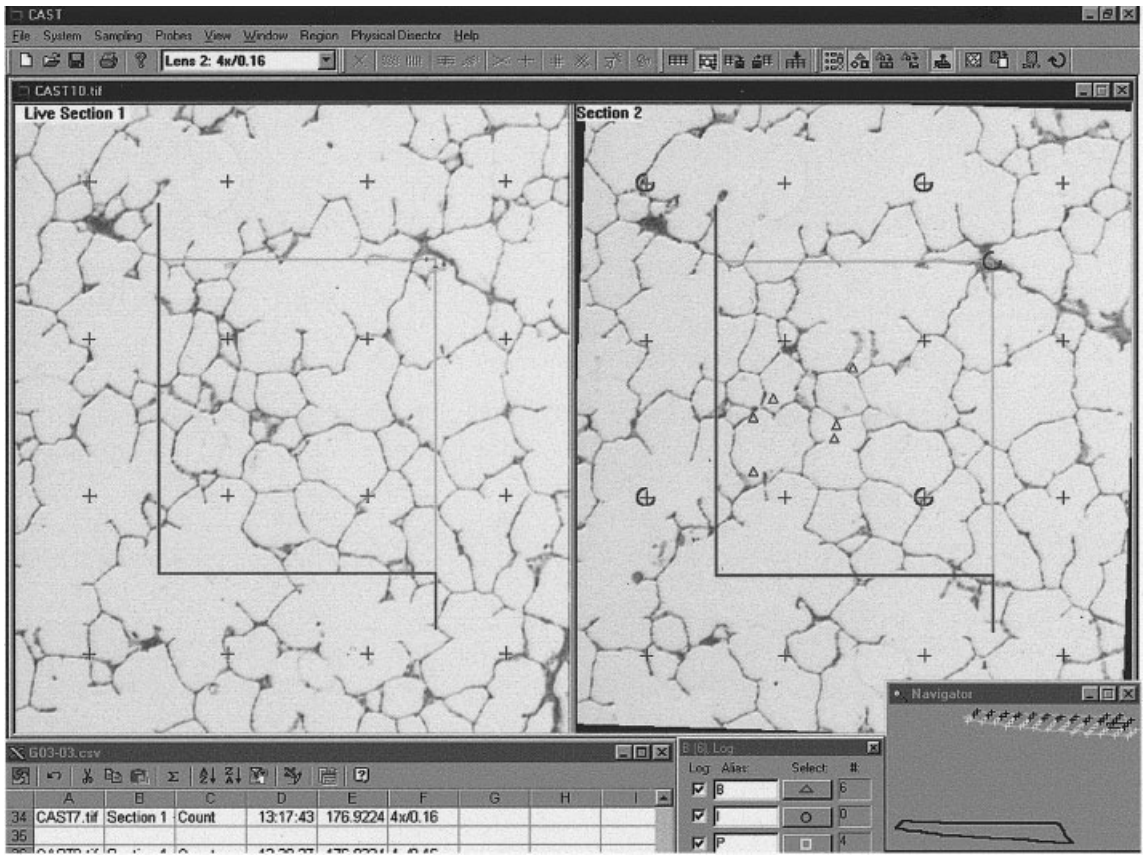

Fig. 8. Counting screen from the CAST system, which has automatically aligned the two corresponding fields from each sections. The unbiased frame is in the middle of each window. The red left and bottom exclusion lines are dark in this grayscale image, the green inclusion lines on the top and right are lightly shaded. Counts (all bridges in the example) are indicated in the right window by Δ. This indicates that a bridge is found in one of the windows and is absent in the other one. At the bottom of the field is part of the spread sheet where the counts are recorded. An outline of the two sections is shown in the lower right corner of the screen. All sampling fields are indicated in the sampling map by crosses, which change color as the fields are sampled.

viously used and the blocks again subsampled according to the fractionator. Samples were selected with a uniformly random start to obtain ~6 blocks. At each step the sampling fraction of tissue was recorded and the blocks were again photographed on millimeter graph paper. As a consequence of the quadratic cross section of bars, the width of processed and embedded and shrunken blocks, BW, is identical to the inaccessible block depth, a quantity one must know for this fractionator design (which avoids exhaustively sectioning of the sampled blocks).

Monkey

Embedding and slicing. The left cranial and left caudal lobes were embedded in agar in a manner similar to the rat lungs. Each lobe was sliced separately according to the IUR protocol, and the slab thickness (usually 18 mm) was selected to obtain 3–6 slices per lobe, from which 5 bars were selected and 4 blocks finally sampled per lobe.

Embedding, Sectioning, and Staining

The sampled blocks of lung tissue were embedded in paraffin using standard protocols. The upper face from the previous sampling step was up in the embedding cassettes so that that face would be sectioned; 5-μm-serial sections were taken using a Leica RM 2155 motor-driven microtome and 2 adjacent serial sections were mounted on one slide. The microtome was calibrated so that the microtome advance, MA, was known. The microtome advance is the reduction of the block height for each cut section: the microtome is calibrated by cutting a large number of sections and measuring directly the total reduction of the block height. A total of four serial sections were taken per block. The sections were stained with hematoxylin and eosin (H&E).

Stereological Estimation

All estimates were made using an Olympus BH-2 microscope with the CAST version 2.00.04 software (Olympus, Denmark). This system consists of a standard upright microscope on which a Prior motorized stage (H101 and H128 3-axis motor controller) is mounted. It is also equipped with a Heidenhain microcator MT-12 gauge with a ND281 measured value display, a JVC 3-CCD KY-F58 color video camera connected to a FlashPoint 3D framegrabber (Integral Technologies, Indianapolis, IN) and a in a Pentium II PC running Windows 98. This is a stereology

15524892, 2004, 1, Downloaded from https://anatomypubs.onlinelibrary.wiley.com/doi/10.1002/ar.a.20012, Wiley Online Library on [17/04/2025]. See the Terms and Conditions (https://onlinelibrary.wiley.com/terms-and-conditions) on Wiley Online Library for rules of use; OA articles are governed by the applicable Creative Commons License

system designed to sample and analyze histological sections correctly for the complete range of stereological techniques.

Physical Disector. Estimation of alveolar number was done by application of the physical disector approach whereby two physically separate sections, a known distance apart, are compared. The first step was to calculate the sampling distance between fields. The field distance must be kept constant throughout all blocks from the same animal and must be known before data collection. To determine the field distance, a trial set of data was run, and the observed features (see below) were counted in a known number of fields. The number of fields needed to obtain a count of roughly 200 for that animal was then calculated (Gundersen et al., 1999) and the sampling distance between fields (Δx and Δy) was then adjusted to obtain about that total number of fields per animal of the given species (cf. Table 1).

The section pair used for the physical disector was separated by one section; sections 1 and 3 or 2 and 4 of the small series were selected based on the technical quality of the section pair. The physical disector height, h(dis), is the distance between the two upper section surfaces, and is therefore twice the microtome advance, MA, in this implementation (Fig. 7).

The two glass slides with the section pair were both put onto the microscope stage. The counting was done by comparing corresponding regions of the two sections. These counts were made using a 4× objective for the monkey and a 10× objective for the rat. First, the CAST system was used to outline the two sections at 1× objective magnification. Fiducial points were then marked on the section pairs to be used by the CAST system for automatic alignment of the corresponding fields in the two sections (using the fiducial markers and all previous alignments, the system also compensates for unequal distortions of the sections). From a 2D random start, the CAST system selected the fields to be analyzed, using the adjusted sampling field distance, described above. For each field, thefirst section image was collected and displayed. This was followed by the CAST system finding the corresponding field of the second section of the pair and viewing that section as a live image displayed together with the still image of the field of the first section (see Fig. 8). A counting frame of known area a(fra) applied to the images represented ~25% of the screen. The fields were counted for bridges, islands, and point hits in the field. Bridges (B) were profiles of interalveolar septum that were complete in one section but incomplete in the other (see Fig. 8). Islands (I) were isolated or unconnected profiles of septum that appeared in one section but not in the other, a very rare event.

Volume Density of Parenchyma and Parenchymal Components

The volume density of parenchymal alveolar air and septa were used in the calculation of alveolar volume (which thus includes the septal volume). The CAST system was also used for this procedure. Sections were outlined for so-called meander sampling of fields and a point set containing 16 points was applied to the section viewed using a 4X objective. Points on non-parenchyma, P(np); parenchymal alveolar air and septa, P(a); and other parenchyma (alveolar duct core air, terminal bronchioles, and their associated vessels), P(o) were counted. Knowing the fractional volume of parenchyma in lung, V_V(par/lung), and that of alveoli and septa in parenchyma lead to the direct estimation of total alveolar volume per lung, V(alv, lung), from the estimated total volume of lung V(lung). Note that V(alv, lung) is independent of global shrinkage (because fractional volume is unchanged by global shrinkage), but is biased by differential shrinkage (not all compartments of the lung shrink equally). This phenomenon was not corrected for in this design, where our main concern is the total number of alveoli. Moreover, the positioning of the invisible separation of alveolar air and the airspace of alveolar duct cannot be unbiased, anyway.

Correction of Global Shrinkage

For the present design for estimating total alveolar number and mean alveolar volume, no correction of global shrinkage is necessary. The correction procedure is only included in order for other studies to use the design for estimates of structural quantities where shrinkage correction must be performed.

In IUR designs, global volume shrinkage is particularly easy to correct for. An unbiased estimate of the global volume change is

$$\text{Shrunken global volume} := (\Sigma SA_{after}/\Sigma BA_{before})^{3/2} \quad (4)$$

where the block area before processing, BA_{before}, is estimated from the photographs and section area after shrinkage, SA_{after}, is estimated by point counting; the summation is over all blocks in an animal. All estimated absolute volumes may now be corrected for global shrinkage by dividing with the above factor—under the explicit assumption that shrinkage is uniform across all tissue components, i.e., there is no differential shrinkage (Dorph-Petersen et al., 2001).

A less precise, but also unbiased estimator of global lineal shrinkage in IUR designs is to compare the BW after and before dehydration and embedding, in analogy to the above Eq. 4. The shrunken global volume is the ratio of linear BWs raised to the third power. Since BW after shrinkage has to be measured for the fractionator estimate of total number, see below, this estimator of global shrinkage was computed (for illustrative purposes only) in this study. Note that Eq. 4 and the above analogue are only valid on IUR sections. In other designs one must estimate volume shrinkage in three orthogonal planes.

Data Calculations

The total number of alveoli in a lung lobe was calculated using the fractionator principle:

$$N(\text{alv,lobe}) := -\chi \quad (5)$$

from Eq. 2, and

$$\chi := \Sigma\Delta\chi\,/SF \quad (6)$$

is the fractionator estimate of the total Euler characteristic of alveolar openings, with $\Delta\chi_3$ from Eq. 3 summed over all disectors and

15524892, 2004, 1, Downloaded from https://anatomypubs.onlinelibrary.wiley.com/doi/10.1002/ar.a.20012, Wiley Online Library on [17/04/2025]. See the Terms and Conditions (https://onlinelibrary.wiley.com/terms-and-conditions) on Wiley Online Library for rules of use; OA articles are governed by the applicable Creative Commons License

$$SF = sf(bar) \cdot sf(block) \cdot sf(height) \cdot sf(area) \quad (7)$$

is the product of all sampling fractions:

sf(bar): the fraction of long bars from the whole lung
sf(block): the fraction of blocks from the long bars
sf(height): the fraction of disector height (2 · MA) in blocks: h(dis)/BW
sf(area): the areal sampling fraction of disectors: a(fra)/($\Delta x \cdot \Delta y$)

The sampling fractions and sampling intensities actually used in this pilot study are shown in Table 1.

Average alveolar volume, $\overline{v_N}(alv)$, is estimated by the defining ratio of total alveolar volume, $\overline{v_N}(alv)$, to the total alveolar number:

$$\overline{v_N}(alv) \equiv \frac{V(alv)}{N(alv)} := \frac{V(lobe)^*V_V(par/lobe)^*V_V(alv/par)}{N(alv, lobe)} \quad (8)$$

Average alveolar diameter: $\overline{d_N} := \sqrt[3]{\frac{6v_N\,(alv)}{\pi}}$ is computed as a crude linear measure of alveolar size under the assumptions that alveoli are spheres and of constant size, both rather unrealistic. But at least the estimate is unaffected by global shrinkage, in this design.

Variance and Efficiency Considerations

For many features of interest in biological tissues, the observed biological variation among individuals is large, and it is useful to know whether it is worth increasing the precision of the stereological sampling or including more animals in the study (Gundersen and Osterby, 1981). One may divide the observed variance (OCV) into its two components, the true biological variation (CV) and the average sampling variation of the stereological measurement (CE) in the following equation for the number of features, N:

$$OCV^2(N) = CV^2(N) + \overline{CE^2}(N) \quad (9)$$

For sensible fractionator sampling designs (Gundersen, 2002) the dominating component of sampling variation is the counting noise. Due to the very sparse sampling the counting noise is rather simple to predict:

$$CE^2_{noise}(N) := 1/(\Sigma B + \Sigma I) \quad (10)$$

where the summation is over one animal. Note that both bridges (B) and islands (I) contribute to the counting noise (but islands count negative in the estimator of number). Other components of sampling variation in fractionator designs are more difficult to predict, as discussed below.

RESULTS

The number of alveoli in the rat ranged from $17.3 \cdot 10^6$ to $24.6 \cdot 10^6$ (mean, CV: $20.1 \cdot 10^6$, 0.15) (cf. Table 3). The right lobe contained 47% more alveoli than the left, a somewhat smaller difference that that of the various volumetric measures of the lobe. The variance among lobes with respect to the total number of alveoli was ~5 times larger (average $CV^2 = 0.33^2$) than that of the total lung: $0.33^2/0.15^2 = 4.8$. The average alveolar volume, $0.50 \cdot 10^6$ μm^3, was identical on the two sides; it corresponds to a (spherical) diameter of ~100 μm. All estimates were independent of animal weight in this rather homogeneous group of retired breeders.

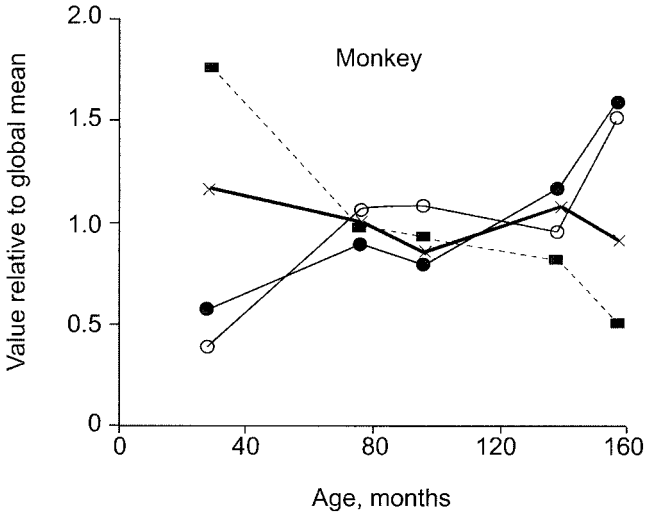

Fig. 9. Estimates from the five monkeys plotted as a function of age. The values are relative to the group mean. Symbols: ×−×: N(alv); ●−●: V(par); ○−○: v(alv); ■—■: N_V(alv/par).

The total number of alveoli in the left lung of the monkey had a mean of $57.8 \cdot 10^6$ and a CV of 0.13, with a range of $48.8 \cdot 10^6$ to $67.4 \cdot 10^6$ (Table 2). Similar to the various volumes, the caudal lobe had more alveoli than the cranial one, on average 36% more. In the monkey, the variance among lobes was of the same order as the variance among left lungs, average CV was 0.16 and 0.13, respectively. The average alveolar volume was $2.93 \cdot 10^6$ μm^3, about six times larger than that of the rat and a bit more than half that of humans (Ochs et al, 2003), with an average (spherical) diameter of ~150 μm. As may be seen from Table 2, all the volumetric measures increased 2- to 3-fold with age, whereas total alveolar number was completely independent of age, which explains why the number of alveoli was clearly much less varying than the volumetric measures in the monkey left lobe (see Fig. 9). The pronounced decrease of the alveolar numerical density (number per mm^3) with age nicely illustrates why numerical densities and changes thereof cannot report total number or changes in this important 0-dimensional quantity.

As expected, the global shrinkage due to dehydration and paraffin embedding was very pronounced: the lung tissue shrank to 34% of the fixed volume in the rat and to 47% in the monkey.

DISCUSSION

Stereological Estimator of Total Alveolar Number

In this study, we used the fractionator (Gundersen, 1986, 2002), a rigorous sampling approach to entire rat lungs and monkey lung lobes, and the Euler characteristic

15524892, 2004, 1, Downloaded from https://anatomypubs.onlinelibrary.wiley.com/doi/10.1002/ar.a.20012, Wiley Online Library on [17/04/2025]. See the Terms and Conditions (https://onlinelibrary.wiley.com/terms-and-conditions) on Wiley Online Library for rules of use; OA articles are governed by the applicable Creative Commons License

to estimate without bias the number of alveoli in rat lungs and monkey lobes. Estimation of the total number of any feature in an organ or any containing space with the fractionator is direct, and there is no need to know the reference volume. This method is unaffected by global and differential shrinkage, swelling and distortion of the containing space during embedding and sectioning.

Our preparation of rat lungs and monkey lobes uses the general principle of support of airway structures by instillation of low-temperature melting agarose (Van Winkle et al., 1996) during lung fixation. We found this method of internal airway support necessary for the uniform cutting of relatively thin slabs of lung tissue in an agarose block prior to further subdivision and smooth fractionator sampling. Other studies have used fractionator sampling to estimate the number of microspheres retained in the lung, but have used triple-fixation by glutaraldehyde, osmium tetroxide, and uranyl acetate, resulting in a very solid lung that allows slabs to be cut at a thickness of 1 mm (Im Hof et al., 1989; Geiser et al., 1990, 1994).

Euler number estimation uses physical disectors that are true volume probes (Sterio, 1984). An advantage of the physical disector is that one can adjust the disector height to achieve the appropriate sample total of 100−200 counts per lung (Gundersen et al., 1999). Euler number estimation of alveoli makes no assumption regarding the size, shape, or orientation of the structures to be counted, in contrast to two-dimensional analyses. In essence, the Euler number count is directed toward counting the rings of alveolar mouth openings. In principle this approach should be valid even with the loss or addition of new interalveolar septa. By contrast, counting alveolar air space indirectly by individual alveolar (biased) volume estimates and volume density of alveoli in parenchymal tissue is extraordinarily time consuming (photographs of ~300 serial sections per stack; Massaro and Massaro, 1992) and thereby an unusually long detour to just number—which may be estimated by simply counting island and bridges in 2 of the ~300 sections. Direct alveolar airspace volume estimation is ironically made impossible by the need to define alveolar mouth openings in three dimensions as a (curved) wall of the alveolar airspace.

The actual counting procedure described in this paper is that of counting discontinuities of a well-defined structure, the alveolar wall. Except for the necessary observer training to concentrate on the ends of the walls, our experience is that the counting is unproblematic in gently processed and nondeflated lung tissue. Artificial disruption of the alveolar walls, as may occur when too viscous agar is instilled or when tissue or sections are damaged, must clearly be avoided.

Optimizing the Sampling Design

Our experience from a number of rats and monkeys lead to some improvements in the sampling design and estimation procedure. The slab thickness in lungs of adult members of the two species might be fixed at 6 and 15 mm, respectively, in order to provide an optimal number of slabs. We would then recommend smooth fractionator sampling (Gundersen, 2002) among all bars and blocks, since it is the most efficient, general sampling paradigm known; it is illustrated in Figure 6. We would recommend section thicknesses in the two species of ~5 and 7 μm, respectively, and the use of adjacent sections.

Because we also wanted to study inhomogeneities among lobes, we counted a total number of events of ~270 per animal. For studies in which just the total number of alveoli is the aim, a total of 100–200 is most likely sufficient. As already indicated, only the counting noise is easily known in fractionator designs. Other components may be kept low by a sensible design (Gundersen, 2002, where their estimation is also described). The estimated CE_{noise} of 0.06 is thus a minimum; the observed total OCV of 0.15 and 0.13 in the two species, respectively, may indicate that the remaining component are indeed low. Since the lung is divided into a constant number of distinct lobes, the choice of reference space for an experiment is an important decision. Using the rat as an example, one may at a first glance have several options:

1. Always the same lung (the left, say)
2. A systematic uniform random lobe (a uniformly random choice of left or right for the first animal, then systematically alternate between left and right for the rest of the group)
3. The whole lung

These options, are however, far from equivalent. The first option only allows biased estimates for the rat (total = 2 · left) because of the systematic side difference and is additionally problematic because changes caused by the experiment may not be symmetrical. The second choice is a simple way of obtaining unbiased estimates (total = 2 · random side, irrespective of systematic side differences). In this particular example, it is, however, rather inefficient because of the pronounced stochastic side difference. Statistically, one would have to use about five times more animals in each group in order to demonstrate a given experimental effect—quite expensive compared to the third option. We emphasize that estimates of variation in small groups are not precise, in reality the ratio of side/total variance of $0.33^2/0.15^2$ may be higher than 4.8 (or smaller, of course).

Regarding the third option, one should not overlook the fact that only a fraction of bars is used, the remaining tissue is a perfect, isotropic, uniformly random sample (with a known sampling fraction) for all other scientific purposes (e.g., stereological, biochemical, immunological).

Number and Sizes of Alveoli

The general description of rat and monkey body weights, ages and lung volumes are similar to previously published values for these species (Fujinaka et al., 1985; Barr et al., 1988; Mercer et al., 1994). A comparative study of cat, dog and rat lungs filled with fluid and air indicate that the density of interalveolar surface forces is the major determinant of lung distensibility in the air-filled state (Haber et al., 1983). In vivo microscopy of a small portion of the ventilatory unit in normal pigs showed little change in alveolar size over most of the pressure volume curve (2–18 mm Hg) (Schiller et al., 2003). In contrast to these observations at the local ventilatory unit level, the distribution of alveolar size in air-filled, frozen dog lungs positioned head up showed a gradient of decreasing size from upper to lower lungs (Glazier et al., 1967). Similarly, a precise morphometric study of regional differences in rat lungs fixed by intratracheal instillation at 20 cm H_2O showed significant decreases in the volume and surface

15524892, 2004, 1, Downloaded from https://anatomypubs.onlinelibrary.wiley.com/doi/10.1002/ar.a.20012, Wiley Online Library on [17/04/2025]. See the Terms and Conditions (https://onlinelibrary.wiley.com/terms-and-conditions) on Wiley Online Library for rules of use; OA articles are governed by the applicable Creative Commons License

densities of interalveolar septa in subpleural compared to central lung regions (Zeltner et al., 1990). These investigators recommended that for quantitative light microscopic analysis of lung tissue, the most appropriate sampling unit is the entire lobe. As indicated above, such a recommendation needs a quantitative basis, however.

The increase in lung volume with age in monkeys is analogous to that in dogs (Hyde et al., 1977). Fisher 344 rats >24 months of age have increased alveolar size (Yamamoto et al., 2003), a result that corresponds with physiological data showing increased airway resistance with aging in Sprague-Dawley rats (Nagase et al., 1994).

Comparison of the absolute numbers of alveoli with published values (Mercer et al., 1994; Massaro and Massaro, 1996) highlight that most investigators have not corrected for tissue shrinkage, a bias that has a dramatic impact on the estimated absolute number of alveoli. Further, considering the variability of alveolar volume with fixation and regional variability within lobes, the very elaborate and indirect method of estimating alveolar number from estimates of alveolar volume and volume density of alveoli within the lung is fraught with bias.

We believe that we have convincingly demonstrated that use of the Euler characteristic with fractionator sampling is a precise, unbiased method for estimation of the number of alveoli in the lung without extensive serial sectioning or three-dimensional reconstruction.

LITERATURE CITED

Barr BC, Hyde DM, Plopper CG, Dungworth DL. 1988. Distal airway remodeling in rats chronically exposed to ozone. Am Rev Respir Dis 137:924–938.

Burri PH. 1984. Fetal and postnatal development of the lung. Annu Rev Physiol 46:617–628.

Dorph-Petersen KA, Nyengaard JR, Gundersen HJ. 2001. Tissue shrinkage and unbiased stereological estimation of particle number and size. J Microsc 204:232–246.

Fujinaka LE, Hyde DM, Plopper CG, Tyler WS, Dungworth DL, Lollini LO. 1985. Respiratory bronchiolitis following long-term ozone exposure in Bonnet Monkeys: a morphometric study. Exp Lung Res 8:167–190.

Geiser M, Cruz-Orive LM, Im HV, Gehr P. 1990. Assessment of particle retention and clearance in the intrapulmonary conducting airways of hamster lungs with the fractionator. J Microsc 160(Pt 1):75–88.

Geiser M, Baumann M, Cruz-Orive LM, Im HV, Waber U, Gehr P. 1994. The effect of particle inhalation on macrophage number and phagocytic activity in the intrapulmonary conducting airways of hamsters. Am J Respir Cell Mol Biol 10:594–603.

Glazier JB, Hughes JMB, Maloney JE, West JB. 1967. Vertical gradient of alveolar size in lungs of dogs frozen intact. J Appl Physiol 23:694–705.

Gundersen HJ. 1986. Stereology of arbitrary particles. A review of unbiased number and size estimators and the presentation of some new ones, in memory of William R. Thompson. J Microsc 143(Pt 1):3–45.

Gundersen HJ. 2002. The smooth fractionator. J Microsc 207:191–210.

Gundersen HJ, Osterby R. 1981. Optimizing sampling efficiency of stereological studies in biology: or "do more less well!" J Microsc 121:65–73.

Gundersen HJ, Bagger P, Bendtsen TF, Evans SM, Korbo L, Marcussen N, Moller A, Nielsen K, Nyengaard JR, Pakkenberg B. 1988a. The new stereological tools: disector, fractionator, nucleator and point sampled intercepts and their use in pathological research and diagnosis. APMIS 96:857–881.

Gundersen HJ, Bendtsen TF, Korbo L, Marcussen N, Moller A, Nielsen K, Nyengaard JR, Pakkenberg B, Sorensen FB, Vesterby A, West MJ. 1988b. Some new, simple and efficient stereological methods and their use in pathological research and diagnosis. APMIS 96:379–394.

Gundersen HJ, Boyce RW, Nyengaard JR, Odgaard A. 1993. The Conneulor: unbiased estimation of connectivity using physical disectors under projection. Bone 14:217–222.

Gundersen HJ, Jensen EB, Kieu K, Nielsen J. 1999. The efficiency of systematic sampling in stereology—reconsidered. J Microsc 193: 199–211.

Haber PS, Colebatch HJH, Ng CKY, Greaves IA. 1983. Alveolar size as a determinant of pulmonary distensibility in mammalian lungs. J Appl Physiol 54:837–845.

Hansen JE, Ampaya EP. 1975. Human air space shapes, sizes, areas, and volumes. J Appl Physiol 38:990–995.

Hyde DM, Robinson NE, Gillespie JR, Tyler WS. 1977. Morphometry of the distal air spaces in lungs of aging dogs. J Appl Physiol 43:86–91.

Im Hof V, Scheuch G, Geiser M, Gebhart J, Gehr P, Heyder J. 1989. Techniques for the determination of particle deposition in lungs of hamsters. J Aerosol Sci 2:247–259.

Karnovsky MJ. 1965. A formaldehyde-glutaraldehyde fixative of high osmolality for use in electron microscopy. J Cell Biol 27:137A-138A.

Massaro GD, Massaro D. 1992. Formation of alveoli in rats: postnatal effect of prenatal dexamethasone. Am J Physiol 263:L37–L41.

Massaro GD, Massaro D. 1996. Formation of pulmonary alveoli and gas-exchange surface area: quantitation and regulation. Annu Rev Physiol 58:73–92.

Mattfeldt T, Mall G, Gharehbaghi H, Moller P. 1990. Estimation of surface area and length with the orientator. J Microsc 159(Pt 3): 301–317.

Mercer RR, Russell ML, Crapo JD. 1994. Alveolar septal structure in different species. J Appl Physiol 77:1060–1066.

Nagase T, Fukuchi Y, Teramoto S, Matsuse T, Orimo H. 1994. Mechanical interdependence in relation to age: effects of lung volume on airway resistance in rats. J Appl Physiol 77:1172–1177.

National Institutes of Health. 1985. Guide for the Care and Use of Laboratory Animals. NIH publication No. 86-23. Revised 1985. Washington, DC: U.S. Government Printing Office.

Ochs M, Nyengaard JR, Jung A, Knudsen L, Wahlers T, Richter J, Gundersen HJG, 2004. The number of alveoli in the human lung. Am J Respir Crit Care Med 169:120–124.

Scherle WF. 1970. A simple method of volumetry of organs in quantitative stereology. Mikroskopie 26:57–60.

Schiller HJ, Steinberg J, Halter J, McCann U, DaSilva M, Gatto LA, Carney D, Nieman G. 2003. Alveolar inflation during generation of a quasi-static pressure/volume curve in the acutely injured lung. Crit Care Med 31:1126–1133.

Sterio DC. 1984. The unbiased estimation of number and sizes of arbitrary particles using the disector. J Microsc 134(Pt 2):127–136.

Thurlbeck WM. 1975. Postnatal growth and development of the lung. Am Rev Respir Dis 111:803–844.

Van Winkle LS, Buckpitt AR, Plopper CG. 1996. Maintenance of differentiated murine Clara cells in microdissected airway cultures. Am J Respir Cell Mol Biol 14:586–598.

Weibel ER. 1963. Morphometry of the human lung. New York: Academic Press.

Weibel ER. 1970. Morphometric estimation of pulmonary diffusion capacity. I. Model and method. Respir Physiol 11:54–75.

Weibel ER, Gomez DM. 1962. A principle for counting tissue structures on random sections. J Appl Physiol 17:343–348.

Yamamoto Y, Tanaka A, Kanamaru A, Tanaka S, Tsubone H, Atoji Y, Suzuki Y. 2003. Morphology of aging lung in F344/N rat: alveolar size, connective tissue, and smooth muscle cell markers. Anat Rec 272A:538–547.

Zeltner TB, Bertacchini M, Messerli A, Burri PH. 1990. Morphometric estimation of regional differences in the rat lung. Exp Lung Res 16:145–158.

15524892, 2004, 1, Downloaded from https://anatomypubs.onlinelibrary.wiley.com/doi/10.1002/ar.a.20012, Wiley Online Library on [17/04/2025]. See the Terms and Conditions (https://onlinelibrary.wiley.com/terms-and-conditions) on Wiley Online Library for rules of use; OA articles are governed by the applicable Creative Commons License